Structural and Mechanical Properties of TTR105-115 Amyloid Fibrils from Compression Experiments

Filip Meersman,[†‡*] Raúl Quesada Cabrera,[‡] Paul F. McMillan,[‡*] and Vladimir Dmitriev[§]
[†]Department of Chemistry, Katholieke Universiteit Leuven, Celestijnenlaan 200F, B-3001 Leuven, Belgium; [‡]Department of Chemistry, University College London, London, United Kingdom; and [§]Swiss-Norwegian Beamlines at ESRF, Boite Postale 220, F-38043 Grenoble, France

ABSTRACT Amyloid fibrils, originally associated with neurodegenerative diseases, are now recognized to have interesting mechanical properties. By using synchrotron x-ray diffraction at high pressure in a diamond anvil cell we determined the bulk modulus of TTR105-115 amyloid fibrils in water and in silicone oil to be 2.6 and 8.1 GPa, respectively. The compression characteristics of the fibrils are quite different in the two media, revealing the presence of cavities along the axis of the fibrils, but not between the β-sheets, which are separated by a dry interface as in a steric zipper motif. Our results emphasize the importance of peptide packing in determining the structural and mechanical properties of amyloid fibrils.

INTRODUCTION

A number of human neurodegenerative diseases, including Alzheimer's disease, type II diabetes, and the prion-related variant Creutzfeldt-Jakob's disease, are characterized by the presence of proteinaceous deposits consisting mainly of amyloid fibrils found among the affected tissue samples. Understanding their formation mechanisms is thus of medical importance. Although only a limited number of proteins are known to form such fibrils in vivo, it is now evident that in vitro, under the right conditions, any polypeptide chain can self-assemble into these fibrillar structures (1). Recently, several groups have also begun to investigate the structure-property relationships in amyloid fibrils for potential nanomaterials applications (2,3). These self-assembled structures possess remarkable mechanical properties that could be harnessed to build and support three-dimensional structures at the nanoscale (2). Their high strength and stability against collapse under compressive loads combined with their potential for functionalization on their external surfaces could lead to new nanodevices (4,5). To develop such applications, it is necessary to learn more about the fibrillar structures and to determine their limits of mechanical resistance and elastic properties.

X-ray diffraction studies of amyloid fibrils indicate they are based on a cross-β motif, in which β-sheets run parallel to the main fibril direction and β-strands lie perpendicular to this axis (6–9). However, the higher-level organization of these structures is variable and has been described by various structural types, including β-sandwich (9) and β-solenoid fold (β-roll or β-helix) models (6,10). Recent crystal-structure determinations of smaller amyloid-forming peptides have now been extrapolated to help interpret fibril-packing arrangements (11,12). The main finding was the existence of a steric zipper structure in which β-strands of one β-sheet interdigitate with those of the opposite β-sheet, thereby creating a dry interface between the sheets. However, this proposal remains to be validated experimentally for amyloid fibrils, and at least one recent study has found differences in peptide packing between crystals and fibrils that could cast doubt on the model (13).

Here, we present synchrotron x-ray diffraction data obtained in situ at high pressure in a diamond anvil cell for mature amyloid fibrils of TTR105-115, an 11-residue peptide corresponding to β-strand G in full-length transthyretin (TTR). The structure adopted by this peptide in the fibril has been elucidated by solid-state NMR (ssNMR) (14). Previous studies on high-pressure stability of TTR105-115 amyloid fibrils indicate that they show remarkable resistance to high pressures extending up to at least 1.0 GPa (15). The results obtained in this study using different pressure-transmitting media (PTM) (H_2O versus silicone oil) permit determination of fibril compressibility and pressure derivative and provide insights into the degree of H_2O incorporation and the amino acid side-chain packing (16,17).

MATERIALS AND METHODS

TTR105-115 peptide was obtained from Eurogentec (Liège, Belgium), and fibrils were prepared as described previously (15). The diffraction pattern at ambient pressure was obtained by measuring a droplet of fibril suspension in a loop. For in situ high-pressure x-ray diffraction measurements, mature amyloid samples were loaded into a diamond anvil cell. In the case where silicone oil was the pressure medium, dried TTR105-115 fibrils were deposited on the diamond surface and a drop of silicone oil (AP100, Fluka, Milwaukee, WI) was added. The sample was contained within a 200-μm hole drilled in a Re gasket. The pressure was determined using the ruby fluorescence method. X-ray diffraction data were collected at the Swiss-Norwegian beamline ($\lambda = 0.7183$ Å) at the European Synchrotron Radiation Facility (Grenoble, France). The sample-to-detector distance and the image-plate inclination angles were calibrated using a LaB_6 standard. All experiments were performed at 22°C. The two-dimensional diffraction

Submitted September 7, 2010, and accepted for publication November 29, 2010.

*Correspondence: filip.meersman@chem.kuleuven.be or p.f.mcmillan@ucl.ac.uk

Editor: Catherine A Royer.

0006-3495/11/01/0193/5 $2.00

doi: 10.1016/j.bpj.2010.11.052

images were azimuthally integrated using the Fit2D program (18), yielding one-dimensional intensity I(s) versus s ($s = d^{-1} = 2\sin\theta/\lambda$, where 2θ is the diffraction angle and λ the wavelength). The peak maxima were determined by peak fitting using PeakFit v4 software (Systat Software, San Jose, CA). The data presented here are based on a single compression experiment, so that the reported error values reflect errors in the fit to the data set rather than any sample variability.

RESULTS AND DISCUSSION

The TTR105-115 fibril diffraction patterns in a capillary and in the diamond anvil cell are shown in Fig. 1. They correspond well those obtained previously for samples studied in aqueous media at ambient pressure (19). Note that no alignment procedures were applied so that the x-ray diffraction patterns represent an isotropic average of fibril orientations in suspension within the H_2O or silicone oil pressure-transmitting fluid environments. The strong signal near 4.7 Å is due to the strand-strand separation along the fiber axis, and this is typically referred to as the meridional reflection in diffraction patterns of aligned samples (8). We also observe the diffuse equatorial 8.8 Å signal due to intersheet distances normal to the fiber axis (19), as well as a 3.8 Å reflection corresponding to C^{α}-C^{α} distances along the peptide backbone (8). These three diffraction peaks were observed throughout the pressure range, confirming the resistance of the fibril structures to high compressive stress environments.

Fig. 2 shows the pressure-induced shift of the main reflections, which allows us to determine the compressibility characteristics of the fibrils that can in turn be interpreted in terms of structural and mechanical properties. The pressure-induced changes in the 4.7-Å, 8.8-Å, and 3.8-Å

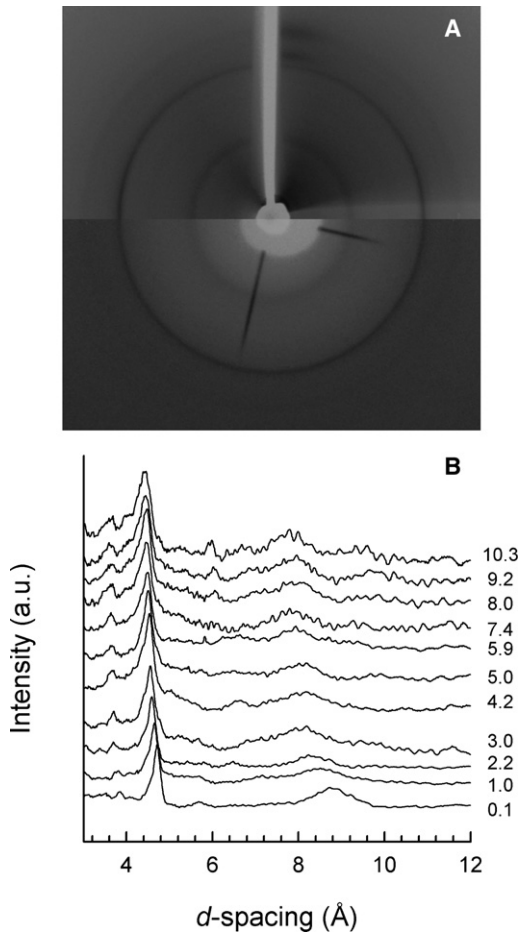

FIGURE 1 X-ray diffraction pattern of TTR105-115 amyloid fibrils in aqueous suspension in the diamond anvil cell. (*A*) Diffraction pattern at ambient pressure in a loop (*upper*) and in the diamond anvil cell (*lower*). (*B*) Integrated and baseline-corrected diffraction patterns in aqueous solution as a function of pressure. The pressure values are indicated in GPa.

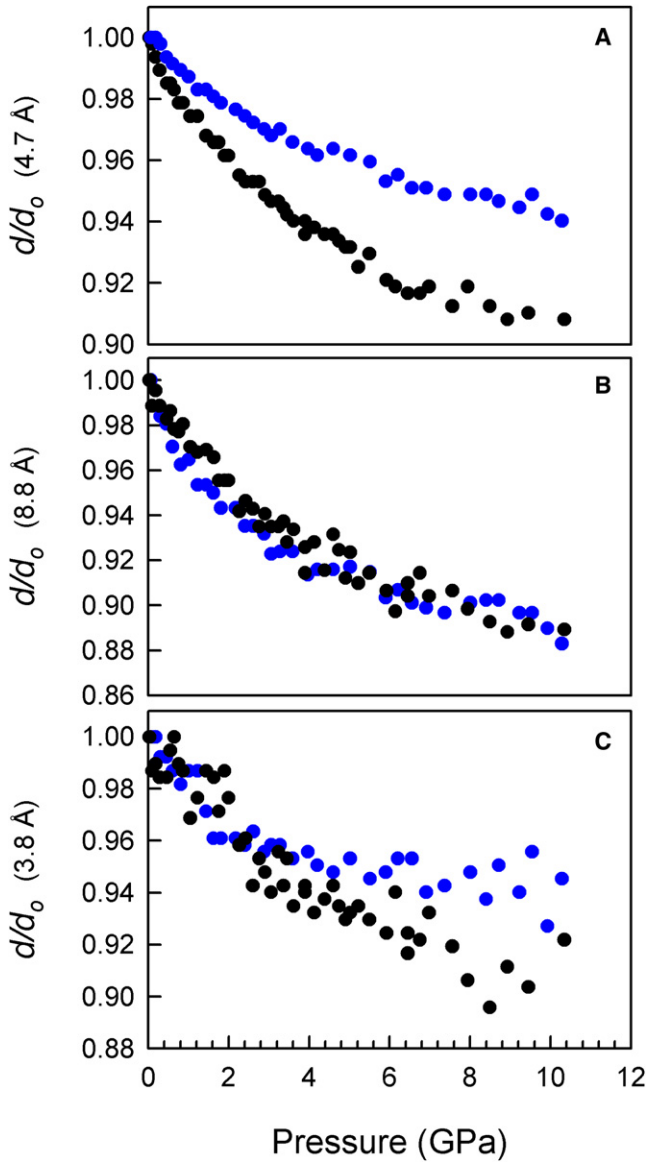

FIGURE 2 Comparison of the pressure dependence of the main fibril reflections in water (*blue*) and silicone oil (*black*). (*A*) Interstrand spacing (4.7 Å). (*B*) Intersheet spacing (8.9 Å). (*C*) C^{α}-C^{α} distance along the peptide backbone (3.8 Å). The standard deviation of the data points is ± 0.003 Å, i.e., less than the size of a dot in the curve.

reflections allow us to determine the compressibility parameters (a, b, c, and V) for a volume element defined along the fibril axis (Fig. 3). We used these data to calculate the bulk modulus (K_o) and its pressure derivative (K_o') using a finite-strain Birch-Murnaghan equation of state expanded to the third order using Eq. 1:

$$P(V) = 3K_o f(1 + 2f)^{5/2}\left(1 + \frac{3}{2}(K_o' - 4)f\right). \quad (1)$$

The volume strain f is given by

$$f = \frac{1}{2}\left[\left(\frac{V}{V_o}\right)^{-2/3} - 1\right] \quad (2)$$

The determined K_o values using water and silicone oil as PTM are 2.6 ± 2.5 and 8.1 ± 0.93 GPa, respectively. These values reflect the bulk modulus of essentially a protofilament consisting of a β-sandwich, and they agree well with estimates

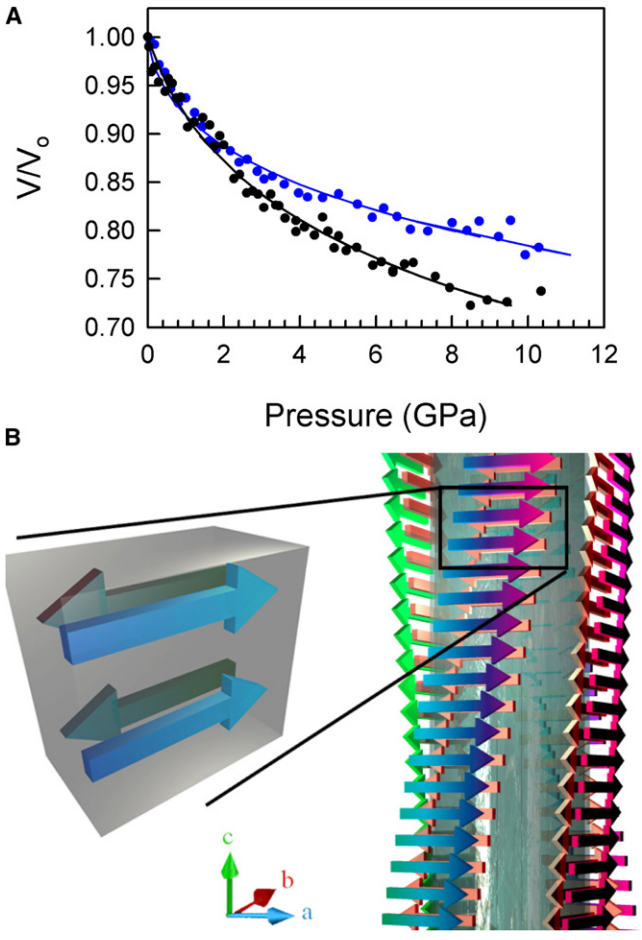

FIGURE 3 Mechanical properties of TTR105-115 fibrils derived from compression experiments. (*A*) Variation of the unit cell volume with pressure in water (*blue*) and silicone oil (*black*). The data (*circles*) have been fit with Eq. 1 (*lines*). (*B*) Schematic representation of a TTR105−115 amyloid fibril showing the assumed unit cell (*left*). The antiparallel orientation of the β-sheets is schematic.

of the elastic moduli derived from atomic force microscopy (AFM) and computer simulation studies on mature fibrils (2). The bulk modulus is mainly determined by the change in the intersheet distance, which shows the largest variation with pressure, in agreement with findings for other layered systems including graphite (20). We note that previous AFM studies and computer modeling yielded an elastic (Young's) modulus along a single dimension under highly nonhydrostatic conditions. However, for most materials including these biological fibrillar structures, the bulk and Young's modulus have similar magnitudes, and the shear modulus is lower by at least an order of magnitude. Our results indicate that the bulk modulus values measured directly using our new approach compare favorably with the Young's modulus obtained from previous AFM studies. If we consider the modulus along the fibril axis obtained from an analysis of the curve in Fig. 2 *A* with the one-dimensional analog of the Murnaghan equation of state (21), then there is also a good agreement between the studies presented here and the AFM results (K_o = 60 ± 3 and 31 ± 1 in water and oil, respectively). Our method therefore provides independent support for the AFM results and also leads to a new strategy for determining elastic properties of fibrillar structures.

Our results emphasize a fundamental difference in compressibility behavior between fibrils observed using H_2O and those observed using silicone oil as the compression medium. The V(P) relations remain indistinguishable until ~1–2 GPa, above which the fibrils compressed in H_2O become substantially less compressible than those mounted in silicone oil (Fig. 3). The change in compressibility can be identified as mainly due to a change in compression behavior along the fibril axis (4.7 Å reflection) (Fig. 2 *A*). This difference cannot be attributed to a phase change in the compression medium. Although liquid water transforms into solid (ice VI) above 1.5 GPa and into ice VII above 2.0 GPa, there are no obvious effects of these phase changes on the compressibility relations of the fibril. In support of this observation, we note that the deviation in compressibility between water and silicone oil can already be seen to begin below 1.5 GPa. The finding that the compressibility is smaller in water than in oil suggests that the fibrils contain small apolar cavities that can be penetrated by water molecules under pressure (22), but not by the larger silicone oil molecules, so that a larger compressibility is observed in the latter case. It is known from solid-state NMR studies that the ends of the peptide are more flexible and do not contribute to the β-strand arrangement (14), whereas Xe incorporation and binding experiments at high pressure have demonstrated the existence of hydrophobic intermolecular sites and exposed pockets within polypeptide fragments (23). Taken together, these results suggest that a few cavities exist within the fibrils that are most likely located outside the cross-β core of the fibrillar structure. Note that the above interpretation assumes that the fibril structure is not affected by the change in PTM from water

to silicone oil. This assumption seems justified given that 1), there is no difference in the positions of the reflections in the two media; and 2), the size of the peptide does not allow it to adopt many other kinds of arrangement without any major changes in the x-ray diffraction pattern.

Comparison of the compression along the fibril axis for TTR105-115 fibers with previous results for insulin fibrils (21) shows that the latter are more compressible. This indicates differences in packing in the two systems, consistent with the idea previously expressed that insulin is a β-solenoid-type structure (10,24), whereas TTR105-115 is more likely to be a β-sandwich-type structure. Moreover, in insulin, which is a larger polypeptide than TTR105-115, structural disorder arising from larger parts of the polypeptide chain outside the fibril core can affect the compressibility. This is in agreement with the observation from AFM measurements that shorter peptides have higher elastic moduli (2). A model for the packing of β_2-microglobulin fibrils, which dissociate at high pressure, also assumed the presence of cavities outside the cross-β core on the basis of density measurements (17). These findings have important implications, as modification or functionalization of amyloid fibrils can significantly alter their mechanical properties and stability, especially if the modification is done before fibril formation, as in the case of hybrid systems (25).

In contrast to the 4.7-Å reflection, the pressure-induced changes in the intersheet distance (8.8-Å reflection) and C^{α}-C^{α} distances (3.8-Å reflection) are independent of the PTM. In the case of the 3.8-Å reflection, there is some scatter at high pressures, but this is likely due to the low intensity and shape of the peak at these pressures. Note that pressure-induced changes in the backbone are in agreement with previous NMR data on BPTI (26). It is interesting to note that the independence of the 8.8-Å reflection on the PTM indicates that no solvent molecules are present between adjacent pairs of β-sheets. This implies that TTR105-115 fibrils are closely packed, and thus provides the first experimental support for a steric zipper motif in amyloid fibrils, as has been suggested for peptide crystals (11,12). The close packing is also inferred from the values of the bulk modulus, which is the reciprocal of the bulk compressibility that is often determined for biological molecules. In an interesting study on a disulfide-bond-deficient variant of lysozyme (HEWL) the partial specific adiabatic compressibilities (β_S) of the protein and its protofibrils were determined from a combination of ultrasound and density measurements (27). It was shown that β_S is -0.075 GPa^{-1} for the disulfide-bond-deficient monomer and 0.0135 GPa^{-1} for the protofibril, suggesting that the latter is more compressible and contains more cavities than the native HEWL, which has a β_S of 0.047 GPa^{-1}. Our bulk modulus values of 2.6 and 8.1 GPa correspond to bulk compressibilities of 0.39 and 0.12 GPa^{-1}, respectively. This indicates that the TTR105-115 amyloid fibrils are less compressible than the average native, globular protein (0.1–0.2 GPa^{-1}) (28) and better packed than HEWL-derived protofibrils. This is consistent with our previous work on TTR105-115, in which we showed that the early (immature) fibrils can be dissociated by pressure, whereas the mature fibrils are pressure-insensitive (15).

CONCLUSIONS

Our results emphasize the importance of peptide packing in addition to the recently highlighted role of hydrogen bonds in fibril formation and stability (2). We have shown previously that TTR105-115 fibrils show a time-dependent change in pressure sensitivity, which was explained in terms of packing changes resulting in fewer cavities and also an increase in the number of hydrogen bonds (15). Efficient packing and optimization of noncovalent interactions also was shown to influence the early stages of the fibril formation process of the GNNQQNY heptapeptide (29). We expect that there should exist a correlation between the mechanical properties and the shape complementarity factor, *Sc*, which was recently found to have a very high value in peptide fibrils (11). Such a correlation would allow the selection of peptide amino acid sequences with desirable mechanical properties.

We thank Dr. Alistair Lennie for scientific support during early experiments carried out at SRS Daresbury and Gines Rivero Hernandez for preparing Fig. 3 *B*.

F.M. is postdoctoral research fellow of the Research Foundation Flanders (FWO-Vlaanderen), Belgium. R.Q.C. was supported by Engineering and Physical Sciences Research Council Senior Research Fellowship EP/D07357X to P.F.M.

REFERENCES

1. Chiti, F., and C. M. Dobson. 2006. Protein misfolding, functional amyloid, and human disease. *Annu. Rev. Biochem.* 75:333–366.
2. Knowles, T. P., A. W. Fitzpatrick, …, M. E. Welland. 2007. Role of intermolecular forces in defining material properties of protein nanofibrils. *Science.* 318:1900–1903.
3. Guo, S., and B. B. Akhremitchev. 2006. Packing density and structural heterogeneity of insulin amyloid fibrils measured by AFM nanoindentation. *Biomacromolecules.* 7:1630–1636.
4. Gras, S. L. 2007. Amyloid fibrils: from disease to design. *Aust. J. Chem.* 60:333–342.
5. Scheibel, T. 2005. Protein fibers as performance proteins: new technologies and applications. *Curr. Opin. Biotechnol.* 16:427–433.
6. Wasmer, C., A. Lange, …, B. H. Meier. 2008. Amyloid fibrils of the HET-s(218-289) prion form a β solenoid with a triangular hydrophobic core. *Science.* 319:1523–1526.
7. Petkova, A. T., Y. Ishii, …, R. Tycko. 2002. A structural model for Alzheimer's β-amyloid fibrils based on experimental constraints from solid state NMR. *Proc. Natl. Acad. Sci. USA.* 99:16742–16747.
8. Blake, C., and L. C. Serpell. 1996. Synchrotron x-ray studies suggest that the core of the transthyretin amyloid fibril is a continuous β-sheet helix. *Structure.* 4:989–998.
9. Jiménez, J. L., J. I. Guijarro, …, H. R. Saibil. 1999. Cryo-electron microscopy structure of an SH3 amyloid fibril and model of the molecular packing. *EMBO J.* 18:815–821.

10. Jiménez, J. L., E. J. Nettleton, …, H. R. Saibil. 2002. The protofilament structure of insulin amyloid fibrils. *Proc. Natl. Acad. Sci. USA.* 99:9196–9201.

11. Sawaya, M. R., S. Sambashivan, …, D. Eisenberg. 2007. Atomic structures of amyloid cross-β spines reveal varied steric zippers. *Nature.* 447:453–457.

12. Nelson, R., M. R. Sawaya, …, D. Eisenberg. 2005. Structure of the cross-β spine of amyloid-like fibrils. *Nature.* 435:773–778.

13. Marshall, K. E., M. R. Hicks, …, L. C. Serpell. 2010. Characterizing the assembly of the Sup35 yeast prion fragment, GNNQQNY: structural changes accompany a fiber-to-crystal switch. *Biophys. J.* 98: 330–338.

14. Jaroniec, C. P., C. E. MacPhee, …, R. G. Griffin. 2004. High-resolution molecular structure of a peptide in an amyloid fibril determined by magic angle spinning NMR spectroscopy. *Proc. Natl. Acad. Sci. USA.* 101:711–716.

15. Dirix, C., F. Meersman, …, K. Heremans. 2005. High hydrostatic pressure dissociates early aggregates of TTR105-115, but not the mature amyloid fibrils. *J. Mol. Biol.* 347:903–909.

16. Meersman, F., and C. M. Dobson. 2006. Probing the pressure-temperature stability of amyloid fibrils provides new insights into their molecular properties. *Biochim. Biophys. Acta.* 1764:452–460.

17. Lee, Y.-H., E. Chatani, …, Y. Goto. 2009. A comprehensive model for packing and hydration for amyloid fibrils of β_2-microglobulin. *J. Biol. Chem.* 284:2169–2175.

18. Hammersley, A. P., S. O. Svensson, …, D. Häusermann. 1996. Two-dimensional detector software: From real detector to idealised image or two-theta scan. *High Pressure Res.* 14:235–248.

19. Squires, A. M., G. L. Devlin, …, C. M. Dobson. 2006. X-ray scattering study of the effect of hydration on the cross-β structure of amyloid fibrils. *J. Am. Chem. Soc.* 128:11738–11739.

20. Hanfland, M., H. Beister, and K. Syassen. 1989. Graphite under pressure: equation of state and first-order Raman modes. *Phys. Rev. B Condens. Matter.* 39:12598–12603.

21. Meersman, F., R. Quesada Cabrera, …, V. Dmitriev. 2009. Compressibility of insulin amyloid fibrils determined by x-ray diffraction in a diamond anvil cell. *High Pressure Res.* 29:665–670.

22. Meersman, F., C. M. Dobson, and K. Heremans. 2006. Protein unfolding, amyloid fibril formation and configurational energy landscapes under high pressure conditions. *Chem. Soc. Rev.* 35:908–917.

23. Colloc'h, N., J. Sopkova-de Oliveira Santos, …, J. H. Abraini. 2007. Protein crystallography under xenon and nitrous oxide pressure: comparison with in vivo pharmacology studies and implications for the mechanism of inhaled anesthetic action. *Biophys. J.* 92:217–224.

24. Choi, J. H., B. C. H. May, …, F. E. Cohen. 2009. Molecular modeling of the misfolded insulin subunit and amyloid fibril. *Biophys. J.* 97: 3187–3195.

25. Baldwin, A. J., R. Bader, …, P. D. Barker. 2006. Cytochrome display on amyloid fibrils. *J. Am. Chem. Soc.* 128:2162–2163.

26. Akasaka, K., H. Li, …, C. K. Woodward. 1999. Pressure response of protein backbone structure. Pressure-induced amide ^{15}N chemical shifts in BPTI. *Protein Sci.* 8:1946–1953.

27. Akasaka, K., A. R. A. Latif, …, K. Gekko. 2007. Amyloid protofibril is highly voluminous and compressible. *Biochemistry.* 46:10444–10450.

28. Ascone, I., R. Kahn, …, R. Fourme. 2010. Isothermal compressibility of macromolecular crystals and macromolecules derived from high-pressure x-ray crystallography. *J. Appl. Cryst.* 43:407–416.

29. Gsponer, J., U. Haberthür, and A. Caflisch. 2003. The role of side-chain interactions in the early steps of aggregation: molecular dynamics simulations of an amyloid-forming peptide from the yeast prion Sup35. *Proc. Natl. Acad. Sci. USA.* 100:5154–5159.